

Evaluation of the Process Parameters on the Microstructure and Mechanical Properties of Cladded SA516 GR70 Steel Welded Joints

H. Ali ¹, Z. Ahmad ², M. Jawad ³, M. W. Hanif ⁴

^{1,2,3,4} Industrial Engineering Department, University of Engineering and Technology Taxila, Pakistan

³ Engr.jawad@uettaxila.edu.pk

Abstract- The current study aims to evaluate the mechanical and microstructure properties of SA516 GR70 medium carbon steel with cladding of stainless-steel SS 316 L using shielded metal arc welding (SMAW) technique. The mechanical and microstructure properties have been evaluated at three process parameters, such as welding electrode material, electrode diameter, and welding current. The ultimate tensile strength (UTS), impact strength, and microhardness (MH) have been selected as output responses. A full factorial design with 27 combinations of experiments has been employed to analyze the effect of process parameters on output responses. Optical microscopy has been used to analyze the microstructure of the welded joints. The analysis of variance (ANOVA) results revealed that the type of welding electrode is found to be the most significant parameter for all three output responses. The 3D mesh contour plots demonstrated that optimal values of UTS of 640 MPa (3.125% improvement from base metal), MH of 380 HV, and impact strength of 115 Joules have been achieved at the experimental settings such as welding electrodes of SS 312, electrode diameter of 3.8 to 4 mm, and welding current ranges of 70 to 90 A. Microstructural analysis revealed that finer austenite grains appeared in the interface region of the joints at the optimal experimental settings, which enhanced the weld mechanical properties. Furthermore, a validation test has shown that mathematical models of these combinations of process parameters and responses are validated due to the low percentage error.

Keywords- Shielded Metal Arc Welding (SMAW); SA516 GR70; Ultimate Tensile Strength; Microhardness and ANOVA.

I. INTRODUCTION

Shielded Metal Arc Welding (SMAW) of steels plays a significant role in highly developed and productive manufacturing sectors, including the

aerospace, locomotive, nuclear-powered, and electric industries [1]. It can be used to join different materials that have superior metallurgical, thermal, and mechanical properties [2]. Due to its essentiality and adaptability, it is used in the fabrication of pressure vessels, separators, heat exchanger shells, pulp digesters, tubes and plates of boilers [3]. SMAW is a process in which heated metals were pounded or slammed together until they fused, which was man's only means for metallurgically uniting metals for generations [4]. However, direct joining of carbon steels is a riskier task due to their low corrosion resistance, which contaminates as well as degrades the other mechanical properties of the welded products [5]. In this regard, coating other materials, specifically stainless steel, on carbon steel is applied, which offers a stain-free welded joint at a low cost that meets the requirements of modern-day industries [6, 7]. In addition, it is common for stainless steel-clad plates to develop cracks-free joints to ensure the safety, integrity, and durability of the equipment [8-9]. However, the selection of appropriate process parameters, electrode materials, and cladding plays a virtual role in avoiding welding defects in the SMAW process.

Researchers studied the effect of different process parameters on the welding joints. For example, Liao [10] conducted a study on the microstructure of a joint comprising AISI 310S and Q235 metals using SMAW. The welding electrodes used were E4303 for the base metal, A102, and A402 for the stainless-steel. The microstructure of the weld specimen consisted of ferrite and pearlite while the cladding weld comprised austenite and white grains. In another study by Qin [11] SAW and SMAW were employed to produce a joint between ASTM TP304 stainless steel-clad steel plate and Q235 carbon steel. ferrite and pearlite grains were observed, while martensite grains formed in the weld close to the stainless-steel cladding. Columnar austenite was observed in the microstructure of the cladding's weld, with skeleton- or worm-like ferrite dispersed. Wang [12] investigated the microstructure and mechanical property of a TIG and SMAW-welded

joint comprising 2205 stainless steel-clad steel plate and 16MnR steel. The study showed that the parent metal of 2205 cladding stainless steel had a microstructure comprising 50.5–58.6 percent ferrite in the heat affected zone (HAZ). The parent metal of the 16MnR base metal contained ferrite and pearlite, with ferrite accounting for 42-54% of the HAZ. Zina [13] investigated the mechanical behavior of 304 stainless steel hot roll cladding. Flahaut has investigated the interface morphology of austenitic stainless steel and low carbon steel hot roll clad plates. Liao [14] utilized (SMAW) to join a Q235 Base metal and an AISI 310S Stainless Steel-metal joint. The welding process involved welding the base metal, transition layer, and stainless-steel cladding in that order. To match the strength and components of each material, Base metal welded with e4303, while A102 and A402 stainless steel electrodes were chosen to weld the conversion level and stainless-steel cladding. The cladding weld primarily comprised single-phase austenite with a small amount of ferrite, whereas the base metal weld and conversion level were mainly composed of ferrite and pearlite microstructures. Furthermore, Wx. [14] studied the effects of three types of welding such as SMAW, tungsten inert gas arc welding process without and with the transition on the mechanical characteristics and microstructure of carbon steel and stainless-steel clade plate joints. They concluded that cladding plate plays virtual role with the transition layer welded joint using the SMAW to gain the optimal UTS (590 MPa) and percentage elongation (47.4%) of Stainless carbon steel and stainless-steel clade plate welded joints. Moreover, the microstructures of titanium-based low-weight metallic materials (TLWMs) that have undergone shielded metal arc welding (SMAW) or tungsten inert gas (TIG) arc welding exhibit a composite composition consisting of both ferrite and austenite phases. Rami [15] examined the microhardness and toughness of the stainless steel-clad plate joint that was manufactured by the hybrid SMAW-GTAW multi-pass welding method. The results indicated that high microhardness values (429 HV) and low toughness (22.9J) were achieved in the vicinity of the local hardening zone that formed on the welded zone after bending tests. However, the process of welding stainless-steel clad plate is considerably more intricate in terms of operational techniques and bonding behavior compared to conventional materials [16-17]. This complexity arises from significant variations in microstructure, chemical composition, and physical and mechanical properties between the cladding metals and the substrate [18-19]. Q [20] examined the microstructural and mechanical properties of stainless steel and carbon steel clad plates joints prepared by the trio of different welding methods such as joining without a changeover coating, welding using tungsten inert gas arc welding, and

welding with a transition layer using SMAW. Results indicated that welded metals in both transition layer cases displayed ferrite and austenite phases due to various solidification modes. However, in the absence of a change layer, extreme diffusion of Cr and Ni led to the creation of a brittle martensite zone in the weld metal. Furthermore, of the three methods tested, SMAW with a transition coating produced the highest quality of welding with minimal dilution of alloy components and no structure of brittle forms, resulting in a flawless welding joint with excellent mechanical properties and no apparent hardness gradient.

From the literature review, it can be inferred that researchers have conducted studies on the welding of different steel grades clad with materials such as Cu, Ni, and stainless steel. The effect of welding process parameters on mechanical and microstructure properties has also been discussed by using different joining methods. However, there is no work reported on joining of clad SA516 GR 70 medium carbon steel through SS 316 L as clad material. The mechanical and microstructure properties of this type of clad joints need to be explored further. It has also been noticed that clad plate joints assist in solving the welding issues and achieving good weld quality, and the microstructural characteristics of weldments [21, 22]. Therefore, the aim of this article is to evaluate mechanical and microstructural properties of clad SA516 GR70 steel welded joints. The effects of three different types of welding electrodes, such as SS 308, SS 316, and SS 309, electrode diameter, and welding current on ultimate tensile strength (UTS), impact strength, and microhardness (MH) have been investigated. A full factorial design has been used to carry out the comprehensive analysis of process parameters in the output response. The analysis of variance (ANOVA) has been carried out to check the significance of each parameter on the output response. The main effects plot analysis has been carried out to check the effect of a single input parameter on output, whereas 3D surface plot analysis has been performed to check the combined effect of two parameters on output. Parametric optimization has been carried out by using contour plot analysis to find the optimal ranges of each parameter against the best output response. The mechanical properties of weld have also been evaluated through microstructure analysis.

II. MATERIALS AND METHODS

Selection of Materials and Experimental Setup

The base metal is selected as medium carbon steel SA516 GR70, and cladding material as stainless-steel SS 316 L. The base metal SA516 GR70 is widely used in pressure vessels and boiler components, especially in drums. For joining

different boiler parts such as plates and tubes, welding has become of prime importance [23]. The chemical composition of plain carbon steel and stainless steel, and mechanical properties of base metals (tensile strength and microhardness) are shown in Table I. After verifying the chemical combination of backing plate material and cladding material through spectroscopy technique, the clad plate has been machined to a size of 19*150*300 mm by a plasma cutting machine. The edges of test samples are prepared using a vertical axis milling machine at 30 degrees and a 1 to 2 mm root face. Two plates have been aligned and tacked together with a 3 mm gap between them prior to welding as per previous studies [24-25]. The faying surfaces of plates have been de-greased and cleaned with acetone to avoid contamination during welding. The welding has been performed on welding inverter machine (LINCOLN INVERTEC V-270T AC/DC). The schematic diagram of the welding process has been shown in Fig. 1.

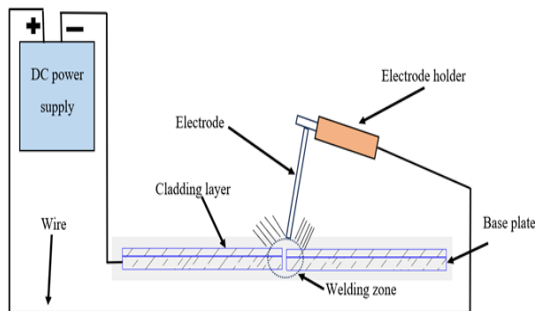


Fig. 1 Schematic of SMAW

Table I: Chemical Composition of Base and Cladding Material, Mechanical Properties of Base Metal

Chemical Composition of Base and Cladded Materials									
Wt. %	C	Mn	Si	Cr	Ni	Mo	P	S	Cu
SA516 GR70	0.03	1.25	1.0	16	14	2.0	0.045	0.03	1.0
SS 316 L	0.27	1.2	0.4	--	--	--	0.035	0.035	--
Mechanical properties of base metal									
Tensile strength = 620 MPa, Microhardness = 355 HV									

Experiment Design

The control process parameters and their levels have been selected based on trial runs and comprehensive literature review. Three levels of selected process parameters are shown in Table II. The values of fixed parameters during welding were measured and taken from the literature review [24-25] as shown in Table III.

Table II: Process Parameters with Three Levels

Process parameters	Levels		
	Lower level	Medium level	Higher level
Welding electrode	SS 308	SS 316	SS 309
Electrode diameter (mm)	2.6	3.2	4
Welding current (A)	55	85	125

Table III: List of Constant Process Parameters and Their Values

Constant Parameters	Values
Root Gap	2.5 mm
Root Face	1-2 mm
Groove Angle	30 degrees
Welding Speed	100 mm/min
Voltage	24 V

The major techniques used to design the experiment and analyses the process parameters included the Response Surface Methodology (RSM), the Taguchi method, and factorial design. It has been observed that RSM does not include any interactive effects among the variables studied and requires a large number of experiments [26]. Similarly, the Taguchi method uses estimates and approximations to achieve target values, and it can be difficult to identify in its own right. Furthermore, it has been determined that the sound-to-noise ratios of the Taguchi method did not consider the full range of external factors [27]. Conversely, full factorial design consists of all combinations of levels for all factors and determine the effects of interactions on the response variable as well [28]. Therefore, a full factorial design has been selected to design the experiments. According to the full factorial design, 27 feasible combinations of experiments have been employed for these process parameters, as shown in Table IV.

Table IV: Experiment Design

Run No.	Process Parameters			Output Response		
	Welding Electrode	Electrode Diameter	Welding Current	Ultimate Tensile Strength (UTS)	Micro-Hardness (HV)	Impact Strength
1	SS 309	3.2	55	590	320	72
2	SS 316	3.2	125	582	332	75
3	SS 309	4	125	569	319	70
4	SS 309	2.5	55	582	332	75
5	SS 308	2.5	55	590	340	83
6	SS 308	4	85	572	322	75
7	SS 308	4	55	592	342	80
8	SS 308	2.5	85	602	352	95
9	SS 316	3.2	55	579	329	72
10	SS 316	2.5	55	602	352	95
11	SS 308	3.2	85	614	364	102
12	SS 309	3.2	125	640	362	110
13	SS 316	4	85	614	364	102
14	SS 309	4	85	623	373	112
15	SS 316	3.2	85	612	362	109
16	SS 309	4	55	628	378	101
17	SS 316	4	55	632	382	115
18	SS 316	4	125	609	359	102
19	SS 308	4	125	620	370	105
20	SS 308	3.2	55	630	362	109
21	SS 308	2.5	125	599	349	99
22	SS 308	3.2	125	612	342	101
23	SS 316	2.5	125	620	370	110
24	SS 309	2.5	85	602	352	99
25	SS 316	2.5	85	622	372	110
26	SS 309	2.5	125	632	382	115
27	SS 309	3.2	85	620	362	110

Mechanical Response Measurement

Mechanical testing is essential for evaluating the fundamental properties of engineering materials, as it affects the design, production, and use of equipment, and ensures the properties of raw

materials used in design and structure. Three tests have been conducted to characterize the mechanical properties of the weldment such as tensile testing, Micro Vicker hardness and Impact Test. According to ASTM E8M standard [29], the tensile sample has been prepared as shown in Fig. 2 (a & b). A tensile testing machine (MTS-810) is used to conduct the tensile tests at a strain rate of 0.1/sec. The Instron Micro Vicker hardness tester is used to measure the micro-Vickers hardness at room temperature having a load of 10 kgf, with a holding time of 10-15 seconds. The Charpy impact test, also known as the Charpy V-notch test is used to conduct the impact test by following ASTM D6110 standard. Metallography has been performed to analyze the microstructure of welded joints. For this, the cross-section of samples has been cut from the welded area through a wire cut electric discharge machine. The samples are grounded through various grits of every paper such as 200 to 2500, then polished through micro cloth. After polishing, the samples are then etched through a glycine solution consisting of 15ml of HCL + 10 ml of glycerin + 5 ml HNO₃.

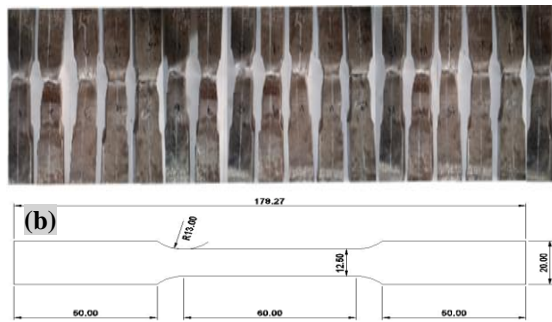


Fig. 2 Tensile testing (a) Tensile test samples (b) ASTM E8M standard.

III. RESULTS AND DISCUSSION

Analysis of Variance (ANOVA) for responses

The Analysis of Variance (ANOVA) has been employed to check the significance of each parameter for the output responses. The ANOVA test has been applied at confidence level of 95% for all responses using Minitab 19.0 software. ANOVA table for UTS (Table V) depicted that model has F-value 3.67, while its p-value (0.033) is lower than 0.05, implies the significance of model. It is worth mention that p-value less than 0.05 indicated model are significant at 95% confidence interval [30-32]. It is also observed that welding electrode has the most significant effect on UTS because of its highest F value in ANOVA table followed by electrode diameter and welding current. The percentage contribution of welding electrode, electrode diameter, and welding current for UTS are 84.10 %, 5.84 %, and 10.06 % respectively. It is also evident from the ANOVA table that interaction has the least effects on the UTS due to its p-value being higher

than 0.05. Furthermore, the value of standard deviation (11.67) and R² (89.20%) show the adequacy of UTS model. In this regard, researchers concluded that higher R Square demonstrated the lower variation of the replications about their mean value [33-34].

Table V: ANOVA for UTS

Source	DF	Adj SS	Adj MS	F-Value	P-Value	% Cont.
Model	18	9003.6	500.20	3.67	0.033	-
Linear	6	8349.1	1391.52	10.21	0.002	-
Welding electrode	2	7020.2	3510.11	25.75	0.000	84.10 %
Electrode diameter	2	488.2	244.11	1.79	0.228	5.84 %
Welding current	2	840.7	420.33	3.08	0.102	10.06 %
2-Way Interactions	12	654.4	54.54	0.40	0.926	-
Welding electrode* Electrode diameter	4	60.9	15.22	0.11	0.975	-
Welding electrode* Welding current	4	439.8	109.94	0.81	0.554	-
Electrode diameter* Welding current	4	153.8	38.44	0.28	0.882	-
Error	8	1090.4	136.31			-
Total	26	10094				-
Model summary						
S	R-Sq.	R-sq (adj.)	R-sq (pred.)			
11.6750	89.20%	64.89%	70.00%			

The analysis of variance (ANOVA) for microhardness reveals that the model exhibits an F-value of 9.10 as shown in Table VI. The percentage contribution of welding electrode, electrode diameter, and welding current for microhardness are 74.77 %, 11.97 %, and 13.26 % respectively. Additionally, the p-value associated with the model is 0.002, which is below the conventional significance level of 0.05. This indicates that the model is statistically significant. Furthermore, it can be noted that the welding electrode exhibits a significant impact on MH, as evidenced by its greatest F value in the ANOVA table. The diameter of the electrode and the magnitude of the welding current exert a substantial influence on the mechanical hardness (MH). The value of standard deviation (7.37174) and R-squared (95.34%) show the adequacy of MH model. It has been determined that R-squared values greater than 90% indicate the adequacy of the statistical model [35]. The ANOVA table provides evidence that the interaction has the least impact on the MH variable, as indicated by its p-value exceeding 0.05.

Table VI: ANOVA for Microhardness

Source	DF	Adj SS	Adj MS	F-Value	P-Value	% Cont.
Model	18	8900.00	494.44	9.10	0.002	-
Linear	6	8450.89	1408.48	25.92	0.000	-
Welding electrode	2	6319.19	3159.59	58.14	0.000	74.77
Electrode diameter	2	1011.63	505.81	9.31	0.008	11.97
Welding current	2	1120.07	560.04	10.31	0.006	13.26
2-Way Interactions	12	449.11	37.43	0.69	0.730	-
Welding electrode* Electrode diameter	4	189.93	47.48	0.87	0.520	-
Welding electrode* Welding current	4	32.81	8.20	0.15	0.957	-
Electrode diameter* Welding current	4	226.37	56.59	1.04	0.443	-
Error	8	434.74	54.34			-
Total	26	9334.74				-
Model Summary						
S	R-Sq	R-sq(adj)	R-sq(pred.)			
7.37174	95.34%	84.86%	46.95%			

The model of impact strength has an F-value of 19.82, according to the analysis of variance (ANOVA) as shown in Table VII. Additionally, the model's p-value is 0.000, which is less than the usual cutoff of 0.05. This demonstrates the statistical significance of the model because it has been mentioned in literature that p-value less than 0.005 depicts the significance of the statistical model [36]. Furthermore, it should be noticed that the welding electrode significantly affects the impact reaction, as shown by the ANOVA table's highest F value for this variable. The welding current strength and electrode diameter both have a significant impact on the impact response. The percentage contribution of welding electrode, electrode diameter, and welding current for impact strength are 88.83 %, 4.03 %, and 7.14 % respectively. The value of standard deviation (4.03228), R-squared (97.81%) show the adequacy and R-square predicted (75.02%) show the accuracy of impact model. The p-value of interaction exceeding 0.05 in the ANOVA table demonstrates that it has the least effect on the impact response.

Table VII: ANOVA for Impact Strength

Source	DF	Adj SS	Adj MS	F-Value	P-Value	% Cont.
Model	18	5800.44	322.25	19.82	0.000	-
Linear	6	5471.78	911.96	56.09	0.000	-
Welding electrode	2	4860.07	2430.0	149.46	0.000	88.83 %
Electrode diameter	2	220.96	110.48	6.79	0.019	4.03 %
Welding current	2	390.74	195.37	12.02	0.004	7.14 %
2-Way Interactions	12	328.67	27.39	1.68	0.234	-
Welding electrode * Electrode diameter	4	98.15	24.54	1.51	0.287	-
Welding electrode * Welding current	4	130.37	32.59	2.00	0.187	-
Electrode diameter * Welding current	4	100.15	25.04	1.54	0.279	-
Error	8	130.07	16.26			-
Total	26	5930.52				-
Model Summary						
S	R-Sq	R-sq(adj)	R-sq (pred.)			
4.03228	97.81%	92.87%	75.02%			

Main Effects Plots

The main effects plot is created using Minitab 19.0 software by showing the means for each value of a category parameter, as illustrated in Fig. 3. It is observed from Fig. 3 (a) that UTS increases significantly as the welding electrode material changes from lower to higher level. The highest UTS value is achieved at Level 2 (SS 309) of welding electrode material. The increase in electrode diameter from Level 1 (2.6 mm) to Level 2 (3.2 mm) causes a considerable decrement in ultimate tensile strength, and then UTS increases with increasing the electrode diameter from 3.2 mm to 4 mm, while the welding electrode depicts the opposite behavior as UTS increases when welding current increases from Level 1 (55 A) to Level 2 (85 A), then with further increase up to Level 3 (125 A), the UTS starts to decrease.

The MH main effects plot showed that MH considerably increases as the welding electrode material changes from a lower to an intermediate level and then starts to decrease at a higher level, as

shown in Fig. 3 (b). The welding electrode material Level 2 (SS 309) achieves the greatest UTS value. A significant rise in MH results from the change in electrode diameter from Level 1 (2.6 mm) to Level 3 (4 mm). Conversely, as the welding current climbs from Level 1 (55 A) to Level 2 (85 A) and then further increases up to Level 3 (125 A), the MH behavior changes from increasing to decreasing. The major effects plot for the impact strength response shows that welding electrodes increase their impact strength value as the welding electrode material transitions from a lower to a middle level as shown in Fig. 3 (c). The welding electrode material exhibits its highest impact value at Level 2 (SS 309). The augmentation of electrode diameter from Level 1 (2.6 mm) to Level 2 (3.2 mm) results in a significant increment in Impact strength response. However, as the electrode diameter is further increased from 3.2 mm to 4 mm, the slope of the increment decreases for Impact strength response. Conversely, the welding current exhibits a contrasting behavior, with the impact strength response increasing as the welding current rises from Level 1 (55 A) to Level 2 (85 A). On the contrary, with a subsequent increase to Level 3 (125 A), the Impact strength response begins to decline.

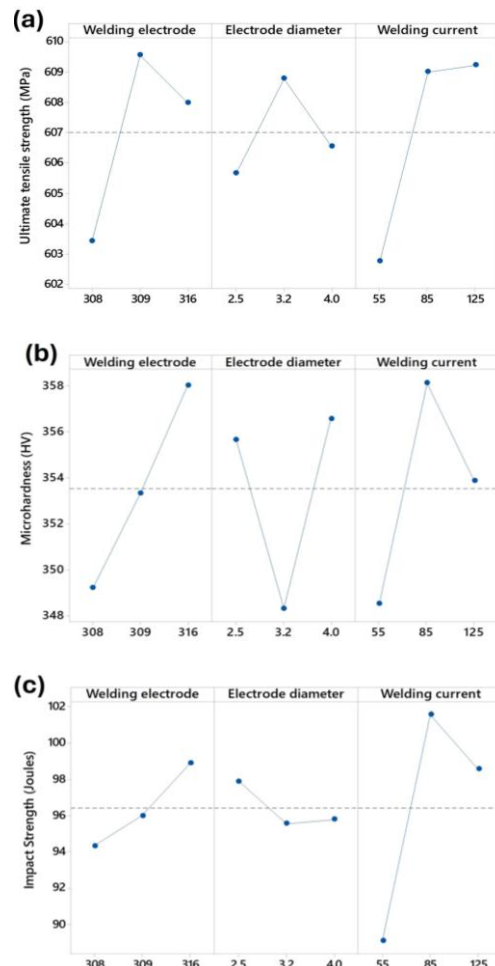


Fig. 3 Main effects plots (a) for UTS (b) for microhardness (c) for Impact strength

3D Surface Plot

The 3D surface plot analysis has been carried out to check the combined effect of two process parameters on the UTS, as shown in Fig. 4 (a–c). The surface plot of electrode diameter versus welding current on the UTS is depicted in Fig. 4(a). It is observed that UTS reduces with increasing electrode diameter from the lower level to the middle level, and then UTS starts increasing with further increase in electrode diameter. The larger diameter electrode causes a larger quantity of melted filler metals in the weld area to fuse the base metals, resulting in an increase in UTS. Similar results have been attained in previous study [37]. Alternatively, UTS increases by raising the welding current from the lower level to middle level and then starts reducing with increases in welding current. The low current causes a lack of penetration, which reduces the strength, whereas an increase in welding current results in better penetration of filler metal, which increases the strength of the weld. Too much high current resulted in spattering defects, which reduced the strength further. The results are well aligned with previous studies [38, 39]. The mesh plot of welding electrode vs. welding current depicts that UTS increases with changing the material of the welding electrode from SS 316 to SS 312 and then gradually decreases with changing the welding electrode material from SS 312 to SS 308, as shown in Fig. 4 (b). At last, the mesh plot of electrode diameter vs. welding electrode depicted that UTS gradually decreased by changing the material of the welding electrode from SS 312 to SS 308, and UTS was observed to be higher at the middle level (3.2 mm) of electrode diameter, as shown in Fig. 4. The larger diameter electrode causes a slower cooling rate that leads to growth of coarser grains which reduced the UTS. Mosaad and Mohamed [40] studies show that the welded region using SS 316 material of welding electrode exhibits a coarse columnar type grains structure, resulting in lower UTS. In contrast, the SS 312 welding electrode material shows longer coarse long grains structure that leads to higher UTS. The 3D surface plots for MH at the various process parameters are depicted in Fig. 5 (a–c). Fig. 5 (a) shows the mesh plot of electrode diameter vs. welding current on the MH. From Fig. 5 (a), it can be shown that MH reduces as electrode diameter grows from the lower level to the intermediate level and then starts to increase as electrode diameter continues to climb up to the upper level. As an alternative, MH rises by raising welding current from a lower level to an intermediate level before beginning to fall with a higher welding current. It is noticeable that the carbon steel HAZ has smaller martensite particles in areas with higher heat input due to high current and finer grains overall, which improves the welded joint's MH [40]. As shown in Fig. 5 (b), the mesh plot of welding electrode vs. welding current showed that MH somewhat

increased as welding electrode material changed from SS 316 to SS 312 and then steadily decreased as welding electrode material changed from SS 312 to SS 308. Finally, the mesh plot of electrode diameter vs. welding electrode in Fig. 5 (c) showed that MH steadily decreased as welding electrode material changed from SS 312 to SS 308, with MH observed to be higher at the middle level of electrode diameter (3.2 mm). The electrode material SS 312 with larger diameter of (3.2 mm) results in finer grain structure which enhances the MH. It is also evident from the Pahlawan [41] studies that fine grain structure found at the welded joints when the 3.2 mm diameter of SS 312 electrode material that leads to enhance the microhardness of ST41 and 316L Stainless Steel welded joints.

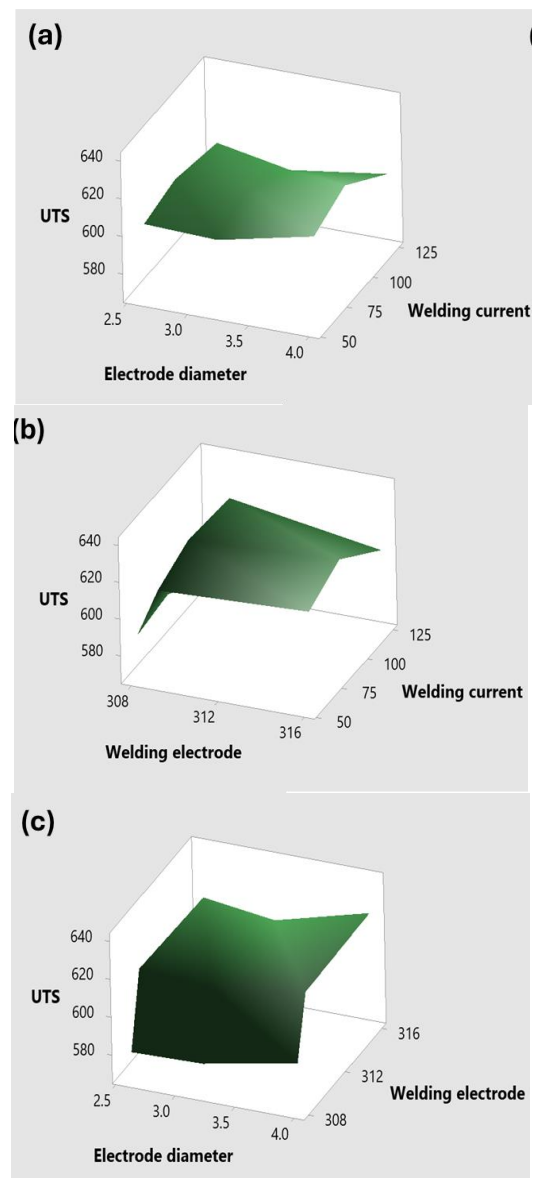


Fig. 4 3D surface plot for evaluating the effect of (a) electrode diameter vs welding current (b) welding electrode vs welding current (c) electrode diameter vs welding electrode for UTS.

The three-dimensional surface plots depicting the combined effect of two process parameters on the impact strength are illustrated in Fig. 6 (a-c). Fig. 6 (a) illustrates the mesh plot representing the relationship between electrode diameter and welding current on the impact strength. The data presented in Fig. 6 (a) demonstrates a clear trend in the impact strength as it relates to the electrode diameter. It is evident that the impact strength has been increased with the increase in the electrode diameter. Lower electrode diameter results in increased heat input and a higher number of welding passes. This consequently causes the grains to become coarser and lowers the impact strength [42]. In an alternative approach, it is seen that the impact strength exhibits an initial rise when the welding current is raised from a lower level to a middle level. The heat input during the welding process is impacted by high current, particularly during the thermal cycle that occurs during heating and cooling. A speedier cooling process is achieved due to the high current input and high heat input. In the welding process, rapid cooling will produce high Impact strength and tensile strength [43]. The mesh plot in Fig. 6 (b) illustrates the relationship between welding electrode material and welding current on impact strength. It is observed that there is a little rise in impact strength when the welding electrode material changes from SS 316 to SS 312. However, a steady decrease in impact strength is observed when the welding electrode material changes from SS 312 to SS 308.

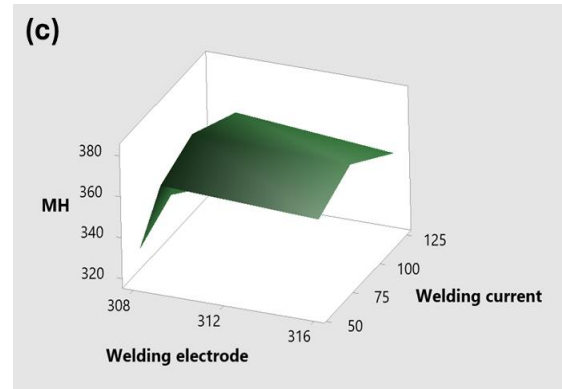
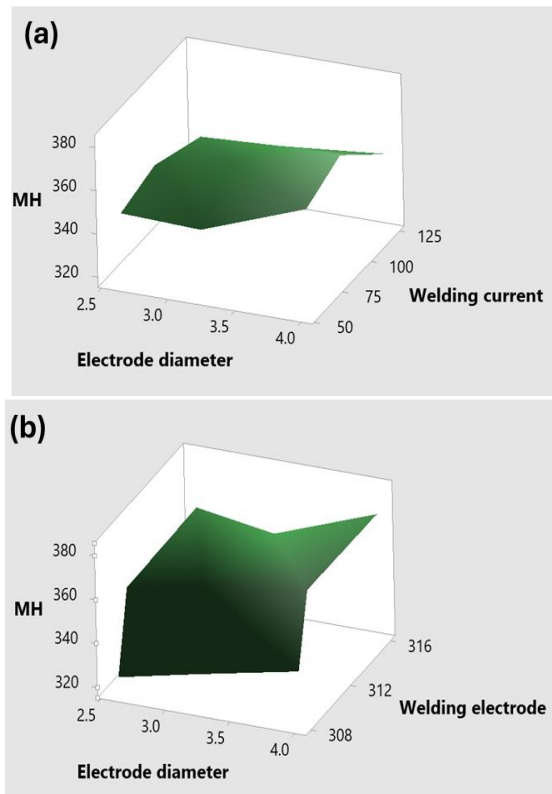
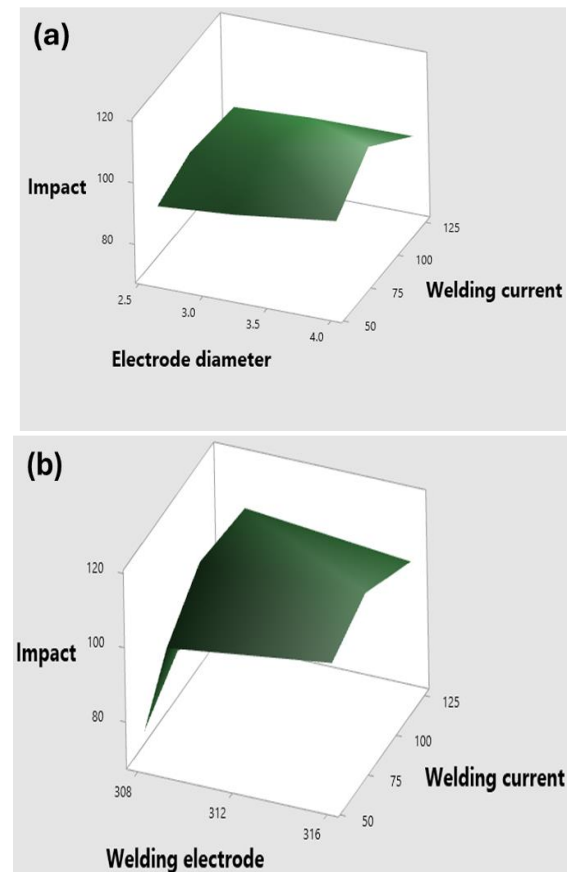


Fig. 5 3D surface plot for evaluating the effect of (a) electrode diameter vs welding current (b) welding electrode vs welding current (c) electrode diameter vs welding electrode for UTS.

Finally, the mesh plot illustrating the relationship between electrode diameter and welding electrode showcases a increase in impact strength while transitioning from a welding electrode material of SS 308 to SS 316. Additionally, it is noted that the impact strength is higher at a moderate level (3.2 mm) of electrode diameter, as illustrated in Fig. 6 (c).



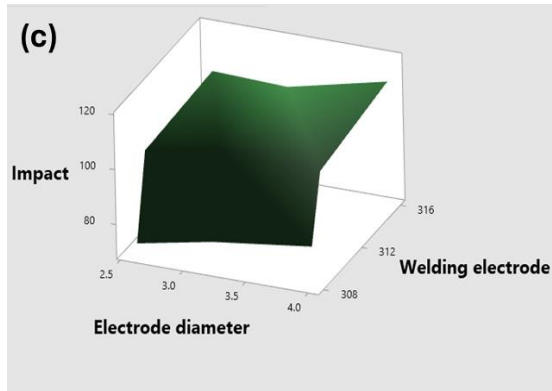


Fig. 6 3D surface plot for evaluating the effect of (a) electrode diameter vs welding current (b) welding electrode vs welding current (c) electrode diameter vs welding electrode for UTS.

The similar trends were attained in the study conducted by Mosaad and Mohamed [40] which proved the changing the electrode material from SS 308 to SS 316 and increase in the electrode diameter from 2.6 mm to 4 mm resulted in a modified grain structure in welded joints and lead to enhanced impact strength.

Analysis of Contour plots

Model-based optimization has been performed using contour plots, which are developed from 3D plots. The contour plot of electrode diameter vs welding current for UTS is shown Fig. 7 (a). The optimum value of UTS (640 MPa) is attained at a range of electrode diameters of 3.8 to 4 mm and a welding current range of 70 to 90 A. The contour plot of welding electrodes against welding current for UTS is shown in Fig. 7 (b). It is found that the optimum value of UTS (640 MPa) is achieved at a welding electrode material from SS 309 to SS 316 with a welding current of 90 to 120 A. The contour plot of electrode diameter vs. welding electrode for UTS is shown in

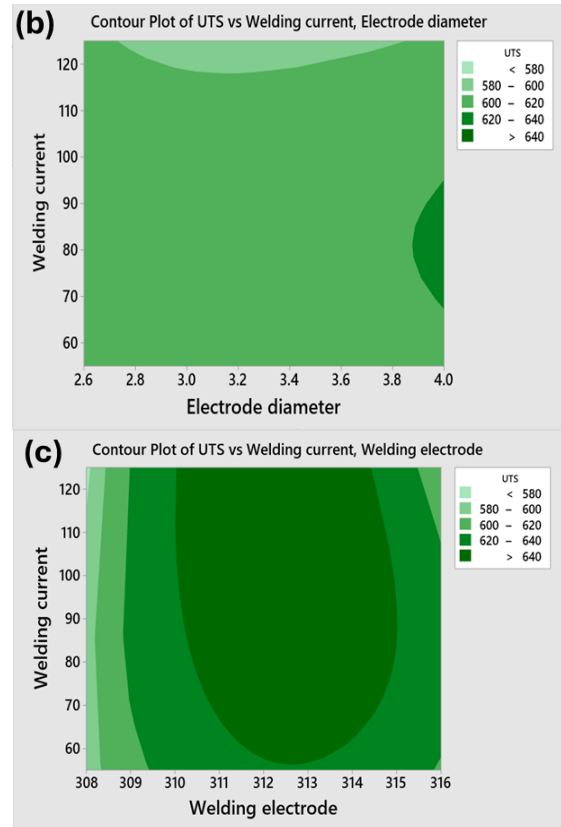
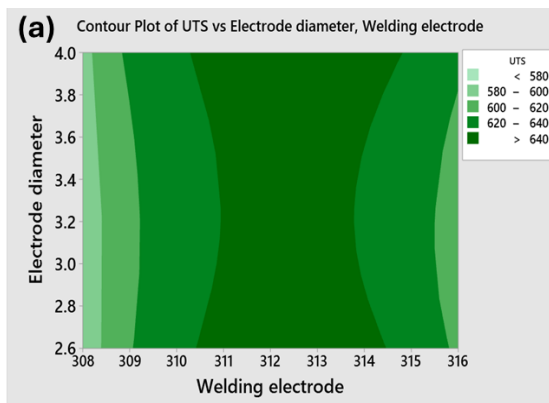


Fig. 7 Contour plot for evaluating the effect of (a) electrode diameter vs welding current (b) welding electrode vs welding current (c) electrode diameter vs welding electrode for UTS.

Fig. 7 (c). It is evident that the optimum value of UTS (640 MPa) is obtained at electrode diameters of 3.2 to 4 mm and welding electrode material from SS 309 to SS 316. The contour plot of electrode diameter vs. welding current for MH is shown in Fig. 8 (a). The optimum value of MH (380 HV) is attained at a range of electrode diameters of 3.8 to 4 mm and a welding current range of 70 to 90 A. The contour plot of the welding electrode against the welding current for MH is shown in Fig. 8 (b). It is found that the optimum value of MH (380 HV) is achieved at a welding electrode material from SS 309 to SS 316 with a welding current of 90 to 120 A. The contour plot of electrode diameter vs. welding electrode for MH is shown in Fig. 8 (c). It is evident that the optimum value of MH (380 HV) is obtained at electrode diameters of 3.2 to 4 mm and welding electrode material from SS 309 to SS 316. The optimal value of impact strength (115 Joules) is reached at an electrode diameter range of 3.8 to 4 mm and a welding current range of 70 to 90 A, as evident in Fig. 9 (a).

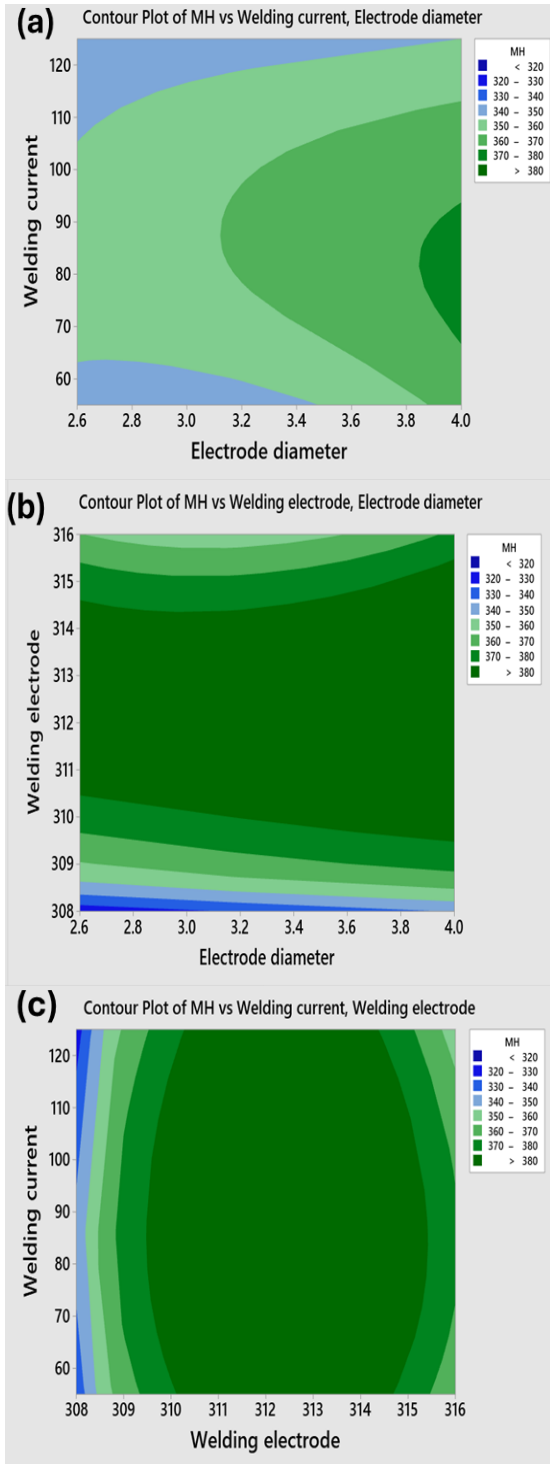


Fig. 8 Contour plot for evaluating the effect of (a) electrode diameter vs welding current (b) welding electrode vs welding current (c) electrode diameter vs welding electrode for MH.

According to Fig. 9 (b), which depicts a contour plot of welding electrodes against vs. welding current for Impact strength, the maximum impact strength value (115 joules) is obtained for welding electrode materials between SS 309 and SS 316 and welding currents between 70 and 90 A. The Impact strength's optimal value (115 joules) is clearly attained at

electrode diameters between 3.8 and 4 mm and welding electrode materials between SS 309 and SS 316, as demonstrated by the contour plot of electrode diameter vs. welding electrode in Fig. 9 (c).

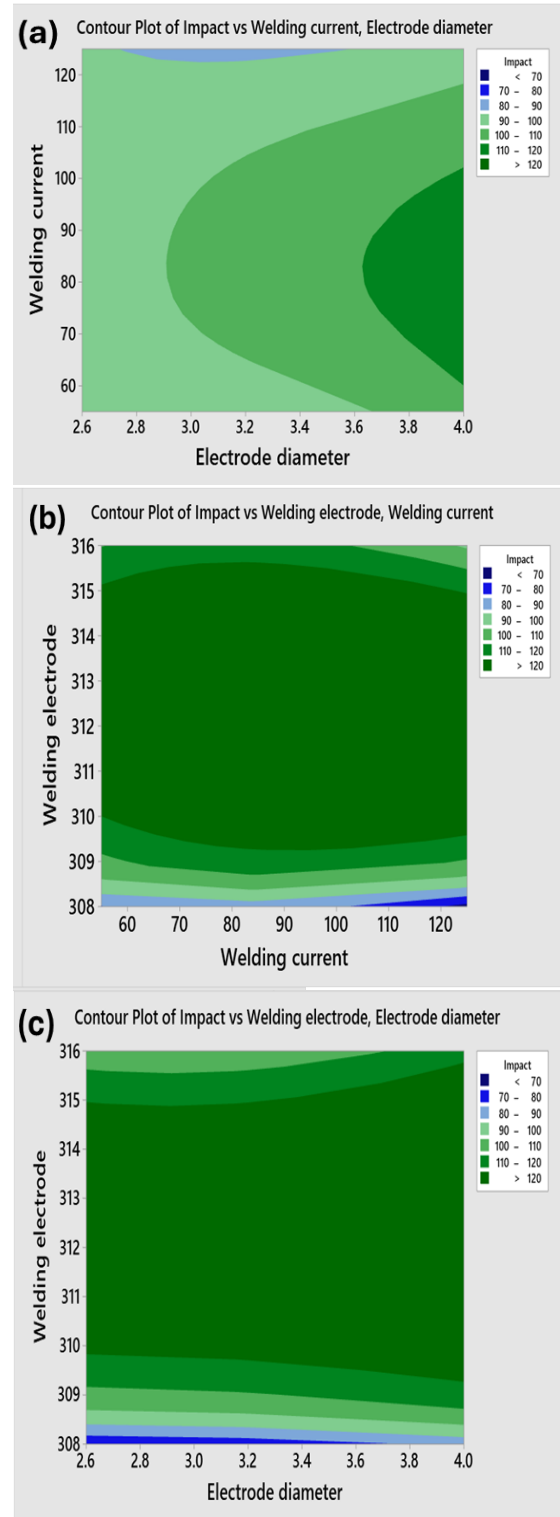


Fig. 9 Contour plot for evaluating the effect of (a) electrode diameter vs welding current (b) welding electrode vs welding current (c) electrode diameter vs welding electrode for Impact strength.

Microstructure Evaluation

The microstructure investigation has been carried out on a welded sample with for the best mechanical properties, at parameters of welding electrode diameter of 3.2 mm and a welding current of 125 A for SS 309. The fusion of base metal SA516 GR70 with cladding of SS 316 L has been shown in Fig. 10. Fig. 10 depicts the different interfaces of base metal and clad material. The microstructure images of fusion zone (zone (a)), fusion zone interface with base metal SA516 GR70 zones (c) and (d), and base metal interface with SS 316 L zone (b) have been shown in Fig. 10 (a-d). The microstructure of weld metal consisted of fine austenite (white regions) and pearlite dendritic grain (dark phases) structure depicted in Fig. 10 (a). This might be the case because stainless-steel filler metal has a significant Impact strength, whereas carbon steel base metal has a negligible one. The micrographic analysis also reveals that the welds have finer austenite grains than the rest due to the improved cooling circumstances at the start of welding; this structure (pearlitic and austenitic) improved the strength of the joint [43]. The micrographic analysis also reveals that the UTS decreases with increasing the electrode diameter from level 2(3.2 mm) to level 3 (4 mm) because welds have finer austenite grains at the 3.2 mm electrode diameter as compared to 4 mm electrode diameter due to the improved cooling circumstances at level 2 of electrode diameter that leads to enhance the UTS of welded joint. It is also evident from Afzal et al [24] studies that electrode having diameter of 4 mm is major causes of slower cooling rate that leads to growth of coarser and larger grain structure. These larger grain structures are more brittle and susceptible to initiating cracks during UTS testing. Similarly, it has been observed that at the optimal experimental conditions, columnar austenite grains structure was observed at the interface of the fusion zone with base materials as shown in Fig. 10 (b). This occurrence is likely due to the lower nucleation energy required at the fusion line and the easier release of welding heat into the fusion zone. As depicted in Fig. 10 (c), the decarburized layer between the stainless steel and the SA516 GR70 base metal forms on the carbon steel side due to element diffusion. The precipitated carbon along the fusion line is seen as a distinct aggregate. Due to the variation of the heat input, it was discovered through microstructural analyses of several strata that there are significant changes in grain size between them. Fig. 10 (d) illustrates the microstructure of the carbon steel HAZ, with ferrite and pearlite (dark grains) being the primary microstructures (bright grains), which increase the hardness as well as impact strength. It can also be observed that the carbon steel HAZ exhibits coarser grains in places with higher heat input and a minor quantity of martensite, which enhances the hardness of welded joint. This could be a result of the alloying

materials eroding from the stainless-steel welds. It is evident from the Mosaad and Mohamed [40] studies that with the change of electrode material from the SS308 to SS316, electrode diameter from 2.6 mm to 4 mm and welding current from the 55A to 85A, grain structure of welded joints that leads to improve the microhardness of welded joints. On the other hand, it has been observed that courser grain structure found at the welded joints leads to reduce the microhardness of welded joints [41].

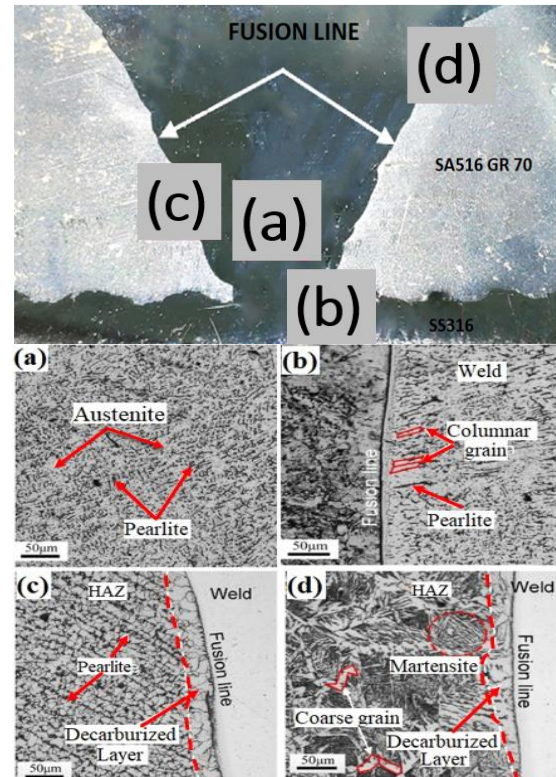


Fig. 10 Microstructure of different zones (a) Weld Metal (b) Stainless Steel Weld (c) Carbon Steel Near to Stainless Steel (d) HAZ of Carbon Steel

IV. EXPERIMENTAL VALIDATION

To check the accuracy of the developed model, validation of the proposed models for each output response has been conducted. In this regard, Wang [44] conducted five experiments in order to validate the mathematical models of surface roughness response developed by the full factorial design and values of process parameters such as cutting speed, feed rate, and depth of cut taken at the middle of the selected levels. Moreover, it has been noticed from the Wang [44] studies that the percentage error between the predicted and actual values below 13%% is acceptable in order to validate the developed mathematical models. Therefore, five experiments have been conducted in this research work to validate the mathematical model of each output response and the values of input process parameters taken between the selected levels of each parameter, as shown in Table VIII.

From Table VIII, it has been determined that percentage errors for each output response is less than 13% and it evident the accuracy of proposed mathematical model for each output response.

Table VIII Experimental Validation

Run	Process parameters			Responses			
	Welding electrode	Electrode diameter (mm)	Welding current (Amp)		Ultimate tensile strength	Micro-Hardness	Impact strength
1	SS 308	2.8	60	Exp.	601	350	102
				Pred.	585	330	95
				% diff.	2.66	5.71	6.86
2	SS 309	3.4	80	Exp.	630	362	130
				Pred.	610	324	119
				% diff.	3.17	10.50	8.46
3	SS 316	3.8	100	Exp.	592	350	101
				Pred.	598	342	96
				% diff.	1.01	2.29	4.95
4	SS 308	3.8	100	Exp.	618	370	125
				Pred.	610	362	119
				% diff.	1.29	2.16	4.80
5	SS 309	2.8	60	Exp.	630	352	110
				Pred.	625	342	105
				% diff.	0.79	2.84	4.55

V. CONCLUSION

The aim of this study is to evaluate the mechanical and microstructural properties of dissimilar joining of SA516 GR70 and SS 316 L. The effects of three different types of welding electrodes, such as SS 308, SS 316, and SS 309, electrode diameter, and welding current on Ultimate tensile strength (UTS), Impact strength, and microhardness (MH) have been investigated. A full factorial design has been used to carry out the comprehensive analysis of process parameters in the output response. The following conclusions have been drawn:

- The ANOVA results show that type of electrode has been the most significant parameter for UTS, MH, and impact strength, whereas electrode diameter is the least significant factor for this response.
- The main effect plots revealed that changing the electrode type of SS 309, electrode diameter of 4 mm, and increase in current of 85 A resulted in an increase in UTS, MH, and impact strength, while the mechanical properties were degraded at the electrode type of SS 308, diameter of 3.2, and current of 125 A.
- The combined effect of electrode diameter vs. welding current shows that the optimum value of UTS of 640 MPa has been attained in the electrode diameter range of 3.8 to 4 mm and the welding current range of 70 to 90 A. The combined effect of electrode material and current revealed an optimized strength of 640

MPa attained at electrode material from SS 309 to SS 316 and a welding current of 90 to 120 A.

- The contour plot of current and electrode diameter has proven that the optimum value of MH of 380 HV is attained at a range of electrode diameters of 3.8 to 4 mm and a welding current range of 70 to 90 A. It is also found that an optimum value of MH of 380 HV is achieved at a welding electrode material from SS 309 to SS 316 and a welding current of 90 to 120 A.
- The optimal value of impact strength of 120 Joules has been achieved at an electrode diameter range of 3.8 to 4 mm and a welding current range of 70 to 90 A, as depicted by the contour plot of electrode diameter vs. welding current. In a contour plot of welding electrode vs. welding current for impact, the best impact strength value (120 joules) is obtained for welding electrode materials between SS 309 and SS 316 and welding currents between 90 and 120 A.
- The fusion zone of the sample with optimal parametric combination shows the austenitic fine grain structure, which enhances the mechanical properties of the weld. The base metal and SS 316 L interface contain columnar grains and a pearlitic structure. The carbon steel HAZ exhibits coarser grains due to higher heat input and a minor quantity of martensite, which enhances the hardness of the weld.

REFERENCES

- [1] Sankarapandian, S., et al., *Microstructure, Mechanical Properties, and Corrosion Behavior of Co-Based Stellite 6 Multilayer Overlays Deposited on ASTM A36 Steel by Gas Metal Arc Welding Process*. steel research international, 2023: p. 2200889.
- [2] Carvalho, G., et al., *Development of optimal deposition strategies for cladding of Inconel 625 on carbon steel using wire arc additive manufacturing*. Surface and Coatings Technology, 2023. 453: p. 129128.
- [3] Song, H., H. Shin, and Y. Shin, *Heat-treatment of clad steel plate for application of hull structure*. Ocean Engineering, 2016. 122: p. 278-287.
- [4] Vijayakumar, S., et al., *Optimization of process variables for shielded metal arc welding dissimilar mild steel and medium carbon steel joints*. Journal of Adhesion Science and Technology, 2023: p. 1-18.
- [5] da Luz, F.S., et al., *Mechanical properties and microstructural characterization of a novel 316L austenitic stainless steel coating on A516 Grade 70 carbon steel weld*. Journal of Materials Research Technology, 2020. 9(1): p. 636-640.

- [6] Matias, J.V., et al., *Behavior of a superaustenitic stainless steel weld cladding deposited by the gas metal arc welding process*. Materials Today Communications, 2023. 34: p. 104978.
- [7] Brandi, S., S. Liu, and R. Thomas, *Electroslag and electrogas welding*. 2011.
- [8] Jing, Y.-a., et al., *A novel reduction-bonding process to fabricate stainless steel clad plate*. Journal of Alloys and Compounds, 2014. 617: p. 688-698.
- [9] Koseki, T., J. Inoue, and S. Nambu, *Development of multilayer steels for improved combinations of high strength and high ductility*. Materials transactions, 2014. 55(2): p. 227-237.
- [10] Liao, H., et al., *Welding process and welded joint microstructure of austenitic stainless clad steel plate*. Hot Work. Technol, 2012. 41: p. 148-150.
- [11] Qin, G., et al., *Microstructures and mechanical properties of stainless steel clad plate joint with diverse filler metals*. Journal of Materials Research and Technology, 2020. 9(2): p. 2522-2534.
- [12] Wang, S.-G., G.-P. Dong, and Q.-H. Ma, *Welding of duplex stainless steel composite plate: influence on microstructural development*. Materials and Manufacturing Processes, 2009. 24(12): p. 1383-1388.
- [13] Dhib, Z., et al., *Cladding of low-carbon steel to austenitic stainless steel by hot-roll bonding: microstructure and mechanical properties before and after welding*. Materials Science and Engineering: A, 2016. 656: p. 130-141.
- [14] Yu, W., et al., *Microstructure and mechanical properties of stainless steel clad plate welding joints by different welding processes*. Science and Technology of Welding and Joining, 2020. 25(7): p. 571-580.
- [15] Ghorbel, R., A. Ktari, and N. Haddar, *Microstructure and mechanical property assessment of stainless steel-clad plate joint made by hybrid SMAW-GTAW multi-pass welding process*. Welding in the World, 2022. 66(8): p. 1593-1608.
- [16] Zhu, Z., et al., *Effect of interface oxides on shear properties of hot-rolled stainless steel clad plate*. Materials Science and Engineering: A, 2016. 669: p. 344-349.
- [17] Kaçar, R. and M. Acarer, *Microstructure-property relationship in explosively welded duplex stainless steel-steel*. Materials Science and Engineering: A, 2003. 363(1-2): p. 290-296.
- [18] Jiang, W., et al., *Influence of repair length on residual stress in the repair weld of a clad plate*. Nuclear Engineering and Design, 2012. 246: p. 211-219.
- [19] Clausmeyer, H. and H. Hantsch, *Manufacture of thick-walled pressure vessels in particular consideration of advanced welding processes and measures for quality assurance*. Nuclear engineering and design, 1991. 129(3): p. 255-276.
- [20] An, Q., et al., *Microstructure and mechanical properties of stainless steel clad plate joints produced by TIG and MAG hybrid welding*. Journal of Adhesion Science and Technology, 2020. 34(6): p. 670-685.
- [21] Kumar, A., A. Bhattacharyya, and C. Pandey, *Structural integrity assessment of Inconel 617/P92 steel dissimilar welds produced using the shielded metal arc welding process*. Journal of Materials Engineering and Performance, 2023: p. 1-19.
- [22] Alipooramirabad, H., et al., *Quenched and Tempered Steels Welded Structures: Modified Gas Metal Arc Welding-Pulse vs. Shielded Metal Arc Welding*. Metals, 2023. 13(5): p. 887.
- [23] Shakya, P., K. Singh, and H.K.J.J.o.P.V.T. Arya, *Influence of External Magnetic Field on Mechanical and Metallurgical Properties of Pressure Vessel Steel (SA 516 Grade 70) Welds Using Gas Tungsten Arc Welding*. 2023. 145(6).
- [24] Afzal, M.S., et al., *Optimization of process parameters for shielded metal arc welding for ASTM A 572 grade 50*. Journal of Engineering Research, 2024.
- [25] Dadi, A., P.B. Goyal, and M.H. Patel, *A review paper on optimization of shielded metal arc welding parameters for welding of (Ms) Sa-516 Gr. 70 plate by using Taguchi approach*. International Journal of Scientific Research in Science and Technology, 2018. 4(5): p. 1536-43.
- [26] Reji, M. and R. Kumar, *Response surface methodology (RSM): An overview to analyze multivariate data*. Indian J. Microbiol. Res, 2022. 9: p. 241-248.
- [27] Roy, R.K., *Design of experiments using the Taguchi approach: 16 steps to product and process improvement*. 2001: John Wiley & Sons.
- [28] Antony, J., *Design of experiments for engineers and scientists*. 2023: Elsevier.
- [29] Jawad, M., et al., *Improvement in mechanical and microstructural properties of novel TA7/Nb/Cu/SS304 composite joints by reducing intermetallic compounds*. 2023: p. 1-18.
- [30] Haider, F., M. Jahanzaib, and M.W. Hanif. *Optimizing the process parameters of Fiction Stir Welded dissimilar 2024Al-5754Al Joint using the Taguchi Method*. in MATEC Web of Conferences. 2023. EDP Sciences.

- [31] Hanif, M.W., et al., *Evaluation of microstructure and mechanical properties of squeeze overcast Al7075– Cu composite joints*. China Foundry, 2023. 20(1): p. 29-39.
- [32] Waseem, M., et al., *Investigating the Ability of Process Parameters to Reduce Defects during the Drilling of Carbon-Fiber-Reinforced Plastic (CFRP) and Aluminum Stack*. Engineering Proceedings, 2023. 45(1): p. 53.
- [33] Hanif, M.W., A. Wasim, and M. Sajid, *Evaluating the Effect of Process Parameters on the Mechanical Properties of an AA7075-Cu Overcast Joint Using the Taguchi Method*. Engineering Proceedings, 2022. 23(1): p. 3.
- [34] Jawad, M., et al., *Performance Evaluation of 70-30 Cu-Ni Filler Metal for Improving Dissimilar Al2024-SS304 Joints' Efficiency: A Mechanical and Microstructural Investigation*. 2023: p. 1-16.
- [35] Imran, A., et al., *Tool Wear Parameter Optimization in Machining a Squeeze-Cast Metal Matrix Composite (Al6061-SiC)*. Engineering Proceedings, 2023. 45(1): p. 1.
- [36] Jawad, M., et al., *Improvement in mechanical and microstructural properties of novel TA7/Nb/Cu/SS304 composite joints by reducing intermetallic compounds*. The International Journal of Advanced Manufacturing Technology, 2023: p. 1-18.
- [37] Suntari, S., et al., *Effect of Electrode Diameter and Current on Dissimilar Metal Welding (Stainless Steel-Galvanized Steel) in Bus Body Construction: Microstructure and Properties Evaluation*. Automotive Experiences, 2022. 5(3): p. 402-415.
- [38] Kiaee, N. and M. Aghaie-Khafri, *Optimization of gas tungsten arc welding process by response surface methodology*. Materials Design, 2014. 54: p. 25-31.
- [39] Jawad, M., et al., *Revealing the microstructure and mechanical attributes of pre-heated conditions for gas tungsten arc welded AISI 1045 steel joints*. International Journal of Pressure Vessels Piping, 2021. 192: p. 104440.
- [40] Mosaad, M. and S. S Mohamed, *Effect of electrode type on the characteristics of AISI 316 Stainless Steel*. Engineering Research Journal-Faculty of Engineering (Shoubra), 2020. 44(1): p. 5-9.
- [41] Pahlawan, I., et al. *Effect of welding electrode variation on dissimilar metal weld of 316l stainless steel and steel ST41*. in *IOP Conference Series: Materials Science and Engineering*. 2021. IOP Publishing.
- [42] Sumardiyanto, D. and S.E. Susilowati, *Effect of welding parameters on mechanical properties of low carbon steel API 5L shielded metal arc welds*. American Journal of Materials Science, 2019. 9(1): p. 15-21.
- [43] Wijoyo, W., et al., *The effect of current strength on tensile strength and impact toughness of cast iron welded joints*. 2021. 17(2): p. 125-130.
- [44] Wang, Z., et al., *Study on surface roughness in high-speed milling of AlMn1Cu using factorial design and partial least square regression*. The International Journal of Advanced Manufacturing Technology, 2015. 76: p. 1783-1792.